

Gradient Flow in Sparse Neural Networks and How Lottery Tickets Win

Utku Evci^{*1}, Yani Ioannou^{*2}, Cem Keskin³, Yann Dauphin¹

¹ Google, ² University of Calgary, ³ Facebook
 evcu@google.com, yani.ioannou@ucalgary.ca, cem.keskin@fb.com, ynd@google.com

Abstract

Sparse Neural Networks (NNs) can match the generalization of dense NNs using a fraction of the compute/storage for inference, and have the potential to enable efficient training. However, naively training unstructured sparse NNs from random initialization results in significantly worse generalization, with the notable exceptions of Lottery Tickets (LTs) and Dynamic Sparse Training (DST). Through our analysis of gradient flow during training we attempt to answer: (1) why training unstructured sparse networks from random initialization performs poorly and; (2) what makes LTs and DST the exceptions? We show that sparse NNs have poor gradient flow *at initialization* and demonstrate the importance of using sparsity-aware initialization. Furthermore, we find that DST methods significantly improve gradient flow *during training* over traditional sparse training methods. Finally, we show that LTs do not improve gradient flow, rather their success lies in re-learning the pruning solution they are derived from — however, this comes at the cost of learning novel solutions.

1 Introduction

Deep Neural Networks (DNNs) are the state-of-the-art method for solving problems in computer vision, speech recognition, and many other fields. While early research in deep learning focused on application to new problems, or pushing state-of-the-art performance with ever larger/more computationally expensive models, a broader focus has emerged towards their efficient real-world application. One such focus is on the observation that only a sparse subset of this dense connectivity is required for inference, as apparent in the success of *pruning*.

Pruning has a long history in Neural Network (NN) literature (Mozer and Smolensky 1989; Han et al. 2015), and remains the most popular approach for finding sparse NNs. Sparse NNs found by pruning algorithms (Han et al. 2015; Zhu and Gupta 2018; Molchanov, Ashukha, and Vetrov 2017; Louizos, Ullrich, and Welling 2017) (i.e. *pruning solutions*) can match dense NN generalization with much better efficiency *at inference* time. However, naively *training* an (unstructured) sparse NN from a random initialization (i.e. *from scratch*), typically leads to significantly worse generalization.

^{*}These authors contributed equally.

Two methods in particular have shown some success at addressing this problem — Lottery Tickets (LTs) and Dynamic Sparse Training (DST). However, we don’t know how to find Lottery Tickets (LTs) efficiently; while RigL (Evci et al. 2020), a recent DST method, requires $5\times$ the training steps to match dense NN generalization. Only in understanding how these methods overcome the difficulty of sparse training can we improve upon them.

A significant breakthrough in training DNNs — addressing vanishing and exploding gradients — arose from understanding gradient flow both at initialization, and during training. In this work we investigate the role of gradient flow in the difficulty of training unstructured sparse NNs from random initializations and from LT initializations. Our experimental investigation results in the following insights:

1. **Sparse NNs have poor gradient flow at initialization.** In §3.1, §4.1 we show that the predominant method for initializing sparse NNs is incorrect in not considering heterogeneous connectivity. We believe we are the first to show that sparsity-aware initialization methods improve gradient flow and training.
2. **Sparse NNs have poor gradient flow during training.** In §3.2, §4.2, we observe that even in sparse NN architectures less sensitive to incorrect initialization, the gradient flow *during training* is poor. We show that DST methods achieving the best generalization have improved gradient flow, especially in early training.
3. **Lottery Tickets don’t improve upon (1) or (2), instead they re-learn the pruning solution.** In §3.3, §4.3 we show that a LT initialization resides within the same basin of attraction as the original pruning solution it is derived from, and a LT solution is highly similar to the pruning solution in function space.

2 Related Work

Pruning Pruning is used commonly in NN literature to obtain sparse networks (Mozer and Smolensky 1989; Han et al. 2015; Kusupati et al. 2020). While the majority of pruning algorithms focus on pruning *after* training, a subset focuses on pruning NNs *before* training (Lee, Ajanthan, and Torr 2019; Wang, Zhang, and Grosse 2020; Tanaka et al. 2020). Gradient Signal Preservation (GRaSP) (Wang, Zhang, and Grosse 2020) is particularly relevant to our study, since

their pruning criteria aims to preserve gradient flow, and they observe a positive correlation between gradient flow *at initialization* and final generalization. However, the recent work of Frankle et al. (2020b) suggests that the reported gains are due to sparsity distributions discovered rather than the particular sub-network identified. Another limitation of these algorithms is that they don’t scale to large-scale tasks like ResNet-50 training on ImageNet-2012.

Lottery Tickets Frankle and Carbin (2019) showed the existence of sparse sub-networks at initialization — known as Lottery Tickets — which can be trained to match the generalization of the corresponding dense DNN. The initial work of Frankle and Carbin (2019) inspired much follow-up work. Liu et al. (2019); Gale, Elsen, and Hooker (2019) observed that the initial formulation was not applicable to larger networks with higher learning rates. Frankle et al. (2019, 2020a) proposed *late rewinding* as a solution. Morcos et al. (2019); Sabatelli, Kestemont, and Geurts (2020) showed that LTs trained on large datasets transfer to smaller ones, but not *vice versa*. Zhou et al. (2019); Frankle, Schwab, and Morcos (2020); Ramanujan et al. (2019) focused on further understanding LTs, and finding sparse sub-networks at initialization. However, it is an open question whether finding such networks at initialization could be done more efficiently than with existing pruning algorithms.

Dynamic Sparse Training Most training algorithms work on pre-determined architectures and optimize parameters using fixed learning schedules. Dynamic Sparse Training (DST), on the other hand, aims to optimize the sparse NN connectivity jointly with model parameters. Mocanu et al. (2018); Mostafa and Wang (2019) propose replacing low magnitude parameters with random connections and report improved generalization. Dettmers and Zettlemoyer (2019) proposed using momentum values, whereas Evci et al. (2020) used gradient estimates directly to guide the selection of new connections, reporting results that are on par with pruning algorithms, and has been applied to vision transformers (Chen et al. 2021), language models (Dietrich et al. 2021), reinforcement learning (Sokar et al. 2021), training recurrent neural networks (Liu et al. 2021b) and fast ensembles (Liu et al. 2021a). In §4.2 we study these algorithms and try to understand the role of gradient flow in their success.

Random Initialization of Sparse NN In training sparse NN from scratch, the vast majority of pre-existing work on training sparse NN has used the common initialization methods (Glorot and Bengio 2010; He et al. 2015) derived for *dense* NNs, with only a few notable exceptions. Liu et al. (2019); Ramanujan et al. (2019); Gale, Elsen, and Hooker (2019) scaled the variance (fan-in/fan-out) of a sparse NN layer according to the layer’s sparsity, effectively using the standard initialization for a small dense layer with an equivalent number of weights as in the sparse model. Lee et al. (2020) measures the singular values of the input gradients and proposes to use a dense orthogonal initialization to ensure dynamical isometry and improve one-shot pruning performance before training. Similar to our work, Tessera, Hooker, and Rosman (2021); Lubana and Dick (2021) compares dense

and sparse networks at initialization and during training using gradient flow, whereas Golubeva, Neyshabur, and Gur-Ari (2021) study the distance to the infinite-width kernel.

3 Analyzing Gradient Flow in Sparse NNs

A significant breakthrough in training very deep NNs arose in addressing the *vanishing/exploding gradient* problem, both at initialization, and during training. This problem was understood by analyzing the signal propagation within a DNN, and addressed in improved initialization methods (Glorot and Bengio 2010; He et al. 2015; Xiao et al. 2018) alongside normalization methods, such as Batch Normalization (BatchNorm) (Ioffe and Szegedy 2015). In our work, similar to Wang, Zhang, and Grosse (2020), we study these problems using gradient flow, $\nabla L(\theta)^T \nabla L(\theta)$ which is the first order approximation* of the decrease in the loss expected after a gradient step. We observe poor gradient flow for the predominant sparse NN initialization strategy and propose a sparsity-aware generalization in §3.1. Then in §3.2 and §3.3 we summarize our analysis of DST methods and the LT hypothesis respectively.

3.1 The Initialization Problem in Sparse NNs

Here we analyze the gradient flow at initialization for random sparse NNs, motivating the derivation of a more general initialization for NN with heterogeneous connectivity, such as in unstructured sparse NNs.

In practice, without a method such as BatchNorm (Ioffe and Szegedy 2015), using the correct initialization can be the difference between being able to train a DNN, or not — as observed for VGG16 in our results (§4.1, Table 1). The initializations proposed by Glorot and Bengio (2010); He et al. (2015) ensure that the output distribution of every neuron in a layer is zero-mean and of unit variance by sampling initial weights from a Gaussian distribution with a variance based on the number of incoming/outgoing connections for all the neurons in a dense layer, as illustrated in Fig. 1a, which is assumed to be identical for all neurons in the layer.

In an unstructured sparse NN however, the number of incoming/outgoing connections is not identical for all neurons in a layer, as illustrated in Fig. 1b. In Appendix B.2 we derive the initialization for this more general case. Here we will focus only on explaining the generalized He et al. (2015) initialization for forward propagation, which we used in our experiments. In Appendix B.1 we explain in full the generalized Glorot and Bengio (2010); He et al. (2015) initialization, in the forward, backward and average use cases.

We propose to initialize every weight $w_{ij}^{[\ell]} \in W^{n^{[\ell]} \times n^{[\ell-1]}}$ in a sparse layer ℓ with $n^{[\ell]}$ neurons, and connectivity mask $[m_{ij}^{[\ell]}] = M^\ell \in [0, 1]^{n^{[\ell]} \times n^{[\ell-1]}}$ with,

$$w_{ij}^{[\ell]} \sim \mathcal{N}\left(0, \frac{2}{fan-in_i^{[\ell]}}\right), \quad (1)$$

where $fan-in_i^{[\ell]} = \sum_{j=1}^{n^{[\ell-1]}} m_{ij}^{[\ell]}$ is the number of incoming connections for neuron i in layer ℓ .

*We omit learning rate for simplicity and ensure different methods have same learning rate schedules when compared.

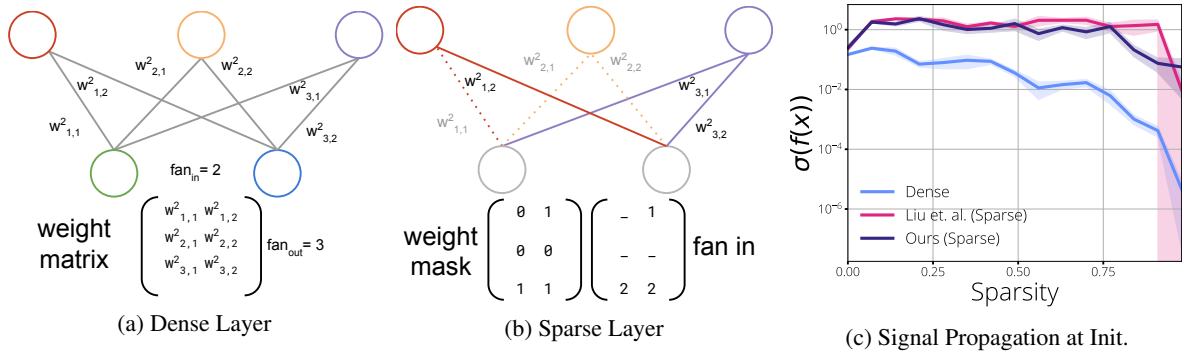


Figure 1: **Glorot/He Initialization for a Sparse NN.** All neurons in a dense NN layer (a) have the same fan-in, whereas in a sparse NN (b) the fan-in can differ for *every neuron*, potentially requiring sampling from a different distribution for every neuron. The initialization derivation/fan-out variant are explained further in Appendix B.1. (c) Std. dev. of the pre-softmax output of LeNet5 with input sampled from a normal distribution, over 5 different randomly-initialized sparse NN for a range of sparsities.

In the special case of a dense layer where $m_{ij}^{[\ell]} = 1, \forall i, j$, Eq. (1) reduces to the initialization proposed by He et al. (2015) since $\text{fan-in}_i^{[\ell]} = n^{[\ell-1]}, \forall i$. Similarly, the initialization proposed by Liu et al. (2019) is another special case where it is assumed $\text{fan-in}_i^{[\ell]} \equiv \mathbb{E}_k[\text{fan-in}_k^{[\ell]}]$, i.e. all neurons have the same number of incoming connections in a layer which is often not true with unstructured sparsity. Using the dense initialization in a sparse DNN causes signal to vanish, as empirically observed in Fig. 1c, whereas sparsity-aware initialization techniques (ours and Liu et al. (2019)) keep the variance of the signal constant.

3.2 Dynamic Sparse Training

While initialization is important for the first training step, the gradient flow during the early stages of training is not well addressed by initialization alone, rather it has been addressed in dense DNNs by normalization methods (Ioffe and Szegedy 2015). Our findings show that even with BatchNorm however, the gradient flow during the training of unstructured sparse NNs is poor.

Recently, a promising new approach to training sparse NNs has emerged — Dynamic Sparse Training (DST) — that learns connectivity adaptively during training, showing significant improvements over baseline methods that use fixed masks. These methods perform periodic updates on the sparse connectivity of each layer: commonly replacing least magnitude connections with new connections selected using various criteria. We consider two of these methods and measure their effect on gradient flow during training: Sparse Evolutionary Training (SET) (Mocanu et al. 2018), which chooses new connections randomly and Rigged Lottery (RigL) (Evci et al. 2019), which chooses the connections with high gradient magnitude. Understanding why and how these methods achieve better results can help us in improving upon them.

3.3 Lottery Ticket Hypothesis

A recent approach for training unstructured sparse NNs while achieving similar generalization to the original dense solution is the Lottery Ticket Hypothesis (LTH) (Frankle and

Carbin 2019). Notably, rather than training a pruned NN structure from random initialization, the LTH uses the dense initialization from which the pruning solution was derived.

Definition [Lottery Ticket Hypothesis]: Given a NN architecture f with parameters θ and an optimization function $O^N(f, \theta) = \theta^N$, which gives the optimized parameters of f after N training steps, there exists a sparse sub-network characterized by the binary mask M such that for some iteration K , $O^N(f, \theta^K * M)$ performs as well as $O^N(f, \theta) * M$, whereas the model trained from another random initialization θ_S , using the same mask $O^N(f, \theta_S * M)$, typically does not*. Initial results of Frankle and Carbin (2019) showed the LTH held for $K = 0$, but later results (Liu et al. 2019; Frankle et al. 2019) showed a larger K is necessary for larger datasets and NN architectures, i.e. $N \gg K \geq 0$.

We measure the gradient flow of LTs and observe poor gradient flow overall. Despite this, LTs enjoy significantly faster convergence compared to regular NN training, which motivates our investigation of the success of LTs beyond gradient flow. LTs require the connectivity mask as found by the pruning solution along with parameter values from the early part of the dense training. Given the importance of the early phase of training (Frankle, Schwab, and Morcos 2020; Lewkowycz et al. 2020), it is natural to ask about the difference between LTs and the solution they are derived from (i.e. pruning solutions). Answering this question can help us understand if the success of LTs is primarily due to its relation to the solution, or if we can identify generalizable characteristics that help with sparse NNs training.

4 Experiments

Here we show empirically that (1) sparsity-aware initialization improves gradient flow at initialization for all methods, and achieves higher generalization for networks without BatchNorm, (2) the mask updates of DST methods increase gradient flow and create new negative eigenvalues in the Hessian; which we believe to be the main factor for improved

*See Frankle et al. (2019) for details. * indicates element-wise multiplication, respecting the mask.

Table 1: **Results of Trained Sparse/Dense Models from Different Initializations.** The initialization proposed in Eq. (1) (Ours) and Liu et al. (2019) improve generalization consistently over masked dense (Original) except for in ResNet50. Note that VGG16 trained without a sparsity-aware initialization fails to converge in some instances. *Baseline* corresponds to the original dense architecture, whereas *Small Dense* corresponds to a smaller dense model with approx. the same parameter count as the sparse models.

	MNIST			ImageNet-2012					
	LeNet5 (95% sparse)			VGG16 (80% sparse)			ResNet50 (80% sparse)		
	Dense	Sparse (Liu)	Sparse (Ours)	Dense	Sparse (Liu)	Sparse(Ours)	Dense	Sparse (Liu)	Sparse (Ours)
Baseline	99.21±0.07			69.25±0.13			76.75±0.12		
Lottery	98.26±0.27			0.10±0.01			75.75±0.12*		
Small Dense	98.21±0.46			61.75±0.09			71.95±0.24		
Scratch	62.99±42.16	96.64±0.83	97.70±0.09	51.81±3.02	62.71±0.05	62.52±0.10	70.58±0.18	70.72±0.16	70.63±0.22
SET	63.33±42.44	97.77±0.31	98.16±0.06	53.55±1.03	63.19±0.26	63.13±0.15	72.93±0.27	72.77±0.27	72.56±0.14
RigL	80.82±34.74	98.14±0.17	98.13±0.09	37.15±26.20	63.69±0.02	63.56±0.06	74.41±0.05	74.38±0.10	74.38±0.01

* With late-rewinding (i.e. $K = 5000$).

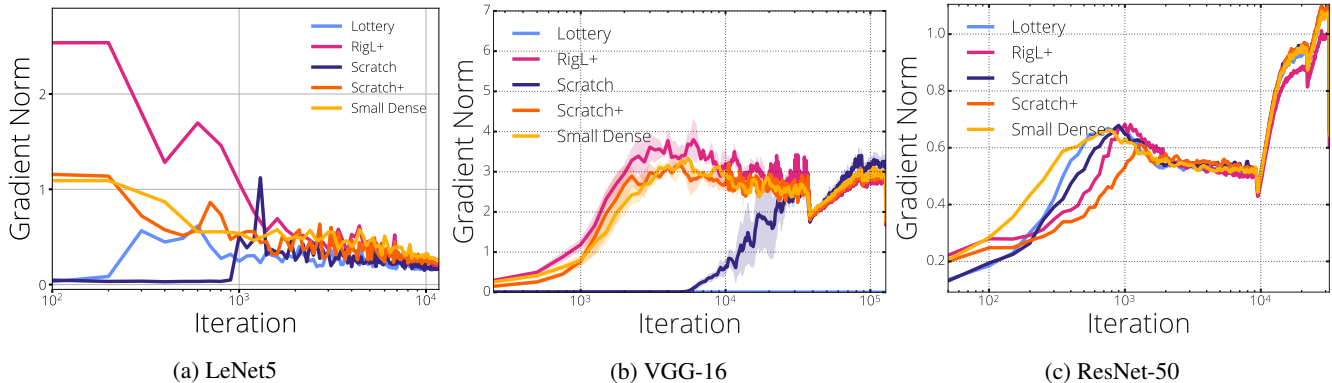


Figure 2: **Gradient Flow of Sparse Models during Training.** Gradient flow during training averaged over multiple runs, ‘+’ indicates training runs with our proposed sparse initialization and Small Dense corresponds to training of a dense network with same number of parameters as the sparse networks. Lottery ticket runs for ResNet-50 include late-rewinding.

generalization, (3) lottery tickets have poor gradient flow, however they achieve good performance by effectively re-learning the pruning solution, meaning they do not address the problem of training sparse NNs in general. Our experiments include the following settings: LeNet5 on MNIST, VGG16 on ImageNet-2012 and ResNet-50 on ImageNet-2012. Experimental details can be found in Appendix A[†].

4.1 Gradient Flow at Initialization

In this section, we measure the gradient flow over the course of the training (Fig. 2) and evaluate the performance of generalized He initialization method (Table 1), and that proposed by Liu et al. (2019), over the commonly used dense initialization in sparse NN. Additional gradient flow plots for the remaining methods are shared in Appendix C. Sparse NNs initialized using the initialization distribution of a dense model (*Scratch* in Fig. 2) start in a flat region where gradient flow is very small and thus initial progress is limited. Learning

[†]Implementation of our sparse initialization, Hessian calculation and code for reproducing our experiments can be found at https://github.com/google-research/rigl/tree/master/rigl/rigl_tf2. Additionally we provide videos that shows the evolution of Hessian during training under different algorithms in the supplementary material.

starts after 1000 iterations for LeNet5 and 5000 for VGG-16, however, generalization is sub-optimal. Liu et al. (2019) reported their proposed initialization has *no empirical effect* as compared to the masked dense initialization[‡]. In contrast, our results show their method to be largely as effective as our proposed initialization, despite the Liu et al. (2019) initialization being incorrect in the general case (see §3.1). This indicates that the assumption of a neuron having roughly uniform connectivity is sufficient for the ranges of sparsity considered, possibly due to a law-of-large-numbers-like averaging effect. We expect this effect to disappear with higher sparsity and our initialization to be more important. Results in Table 2 for a 98% sparse LeNet5 demonstrate this, in which our sparsity-aware initialization provides 40% improvement on test accuracy. Our initialization remedy the vanishing gradient problem at initialization (*Scratch+* in Fig. 2) and result in better generalization for all methods. For instance, improved initialization results in an 11% improvement in Top-1 accuracy for VGG16 (62.52 vs 51.81). While initialization is extremely important for NNs without BatchNorm and skip connections, its effect on modern architectures, such

[‡]Models with BatchNorm and skip connections are less affected by initialization, and this is likely why the authors did not observe this effect.

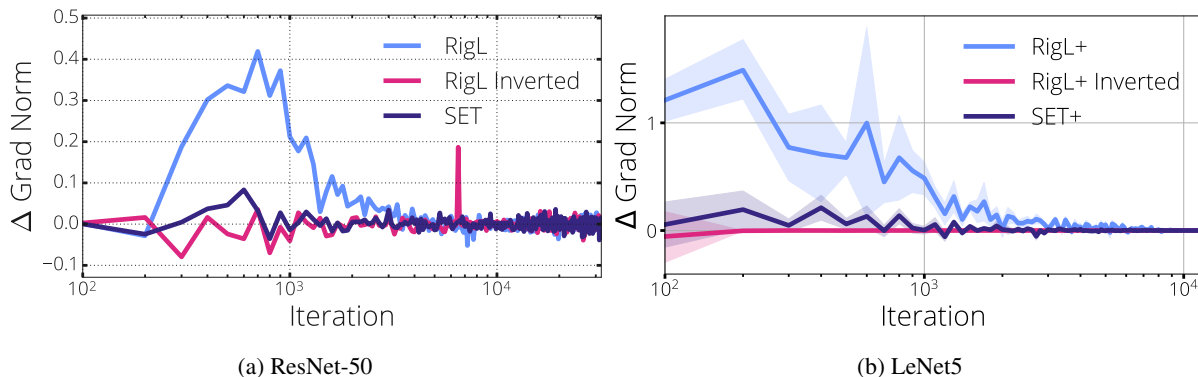


Figure 3: **Effect of Mask Updates in Dynamic Sparse Training.** Effect of mask updates on the gradient norm. *RigL Inverted* chooses connections with least magnitude. We measure the gradient norm before and after the mask updates and plot the Δ . ‘+’ indicates proposed initialization and used in MNIST experiments.

	Dense/Other	Sparse (Liu)	Sparse (Ours)
Scratch	11.35±0.00	56.51±36.90	90.00±4.04
RigL	11.35±0.00	62.34±41.63	96.72±0.23
Prune	96.50±0.31	–	–

Table 2: **Sparsity-aware Initialization and Generalization: Sparse (98%) LeNet5 (MNIST).** Results show the importance of our sparsity-aware initialization at higher sparsity regimes, compared with a standard dense initialization (He et al. 2015), or scaled-sparse initialization (Liu et al. 2019).

as Resnet-50, is limited (Evci et al. 2019; Zhang, Dauphin, and Ma 2019; Frankle et al. 2020b). We confirm these observations in our ResNet-50 experiments in which, despite some initial improvement in gradient flow, sparsity-aware initializations seem to have no effect on final generalization. Additionally, we observe significant increase in gradient norm after each learning rate drop (due to increased gradient variance), which suggests studying the gradient norm in the latter part of the training might not be helpful.

The LT hypothesis holds for MNIST and ResNet50 (when $K=5000$) but not for VGG16. We observe poor gradient flow for LTs at initialization similar to *Scratch*. After around 2000 steps gradients become non zero for *Scratch*, while gradient flow for LT experiments stay constant. Our sparse initialization improves gradient flow at initialization and we observe a significant difference in gradient flow during early training between RigL and Scratch+. DST methods alone can help resolve gradient flow problem at initialization and thus bring better performance. This is reflected in Table 1: Scratch, SET and RigL obtains 63%, 63% and 81% respectively; all starting from the bad initialization (Dense).

4.2 Gradient Flow During Sparse Training

Our hypothesis for Fig. 2 is that the DST methods improve gradient flow through the updates they make on the sparse connectivity, which in turn results in better performance. To verify our hypothesis, we measure the change in gradient flow and Hessian spectrum whenever the sparse connectiv-

ity is updated. We also run the inverted baseline for RigL (*RigL Inverted*), in which the growing criteria is reversed and connections with the *smallest* gradients are activated as in Frankle et al. (2020b).

DST methods such as RigL replace low saliency connections during training. Assuming the pruned connections indeed have a low impact on the loss, we might expect to see increased gradient norm after new connections are activated, especially in the case of RigL, which picks new connections with high magnitude gradients. In Fig. 3 we confirm that RigL updates increase the norm of the gradient significantly, especially in the first half of training, whereas SET, which picks new connections randomly, seems to be less effective at this. Using the inverted RigL criteria doesn’t improve the gradient flow, as expected, and without this RigL’s performance degrades (73.83 ± 0.12 for ResNet-50 and 92.71 ± 7.67 for LeNet5). These results suggest that improving gradient flow early in training — as RigL does — might be the key for training sparse networks. Various recent works that improve DST methods support this hypothesis: longer update intervals Liu et al. (2021c) and adding parallel dense components (Price and Tanner 2021) or activations (Curci, Mocanu, and Pechenizkiy 2021) that improve gradient flow brings better results. Additional plots (Appendix C) using different initialization methods demonstrate the same behaviour.

When the gradient is zero, or uninformative due to the error term of the approximation, analyzing the Hessian could provide additional insights (Sagun et al. 2017; Ghorbani, Krishnan, and Xiao 2019; Pappas 2019). In Appendix E, we show the Hessian spectrum before and after sparse connectivity updates. After RigL updates we observe more negative eigenvalues with significantly larger magnitudes as compared to SET. Large negative eigenvalues can further accelerate optimization if corresponding eigenvectors are aligned with the gradient. We leave verifying this hypothesis as a future work.

4.3 Why Lottery Tickets are Successful

We found that LTs do not improve gradient flow, either at initialization, or early in training, as shown in Fig. 2. This may be surprising given the apparent success of LTs, however the

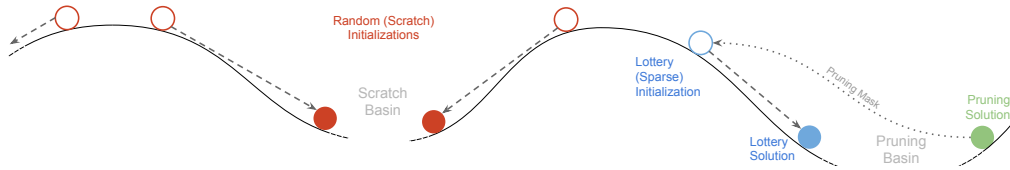


Figure 4: **Lottery Tickets Are Biased Towards the Pruning Solution, Unlike Random Initialization.** A cartoon illustration of the loss landscape of a sparse model, after it is pruned from a dense solution to create a LT sub-network. A LT initialization is within the basin of attraction of the pruned model’s solution. In contrast a random initialization is unlikely to be close to the dense solution’s basin.

questions posed in §3.3 present an alternative hypothesis for the ease of training from a LT initialization: Can the success of LTs be due to their relationship to well-performing pruning solutions? Here we present results showing that indeed (1) LTs initializations are consistently closer to the pruning solution than a random initialization, (2) trained LTs (i.e. LT solutions) consistently end up in the same basin as the pruning solution and (3), LT solutions are highly similar to pruning solutions under various function similarity measures. Our resulting understanding of LTs in the context of the pruning solution and the loss landscape is illustrated in Fig. 4.

Experimental Setup To investigate the relationship between the pruned and LT solutions we perform experiments on two models/datasets: a 95% sparse LeNet5[§] architecture (LeCun et al. 1989) trained on MNIST (where the original LT formulation works, i.e. $K = 0$), and an 80% sparse ResNet-50 (Wu, Zhong, and Liu 2018) on ImageNet-2012 (Russakovsky et al. 2015) (where $K = 0$ doesn’t work (Frankle et al. 2019)), for which we use values from $K = 2000$ ($\approx 6^{\text{th}}$ epoch). In both cases, we find a LT initialization by pruning each layer of a dense NN separately using magnitude-based iterative pruning (Zhu and Gupta 2018). Further details of our experiments are in Appendix A.

Lottery Tickets Are Close to the Pruning Solution We train 5 different models using different seeds from both *scratch* (random) and LT initializations, the results of which are in Figs. 5b and 5e. These networks share the same pruning mask and therefore lie in the same solution space. We visualize distances between initial and final points of these experiments in Figs. 5a and 5d using 2D Multi-dimensional Scaling (MDS) (Kruskal 1964) embeddings. **LeNet5/MNIST:** In Fig. 5b, we provide the average L2 distance to the pruning solution at initialization (d_{init}), and after training (d_{final}). We observe that LT initializations start significantly closer to the pruning solution on average ($d_{init} = 13.61$ v.s. 17.46). After training, LTs end up more than $3\times$ closer to the pruning solution compared to scratch. **Resnet-50/ImageNet-2012:** We observe similar results for Resnet-50/ImageNet-2012. LTs, again, start closer to the pruning solution, and solutions are $5\times$ closer ($d_{final} = 39.35$ v.s. 215.98). These results explain non-random initial loss values for LT initializations (Zhou et al. 2019) and their inability to find good solutions if repelled by pruning solutions (Maene, Li, and Moens 2021). LTs are biased towards the pruning solution they are derived

[§]Note: We use ReLU activation functions, unlike the original architecture (LeCun et al. 1989).

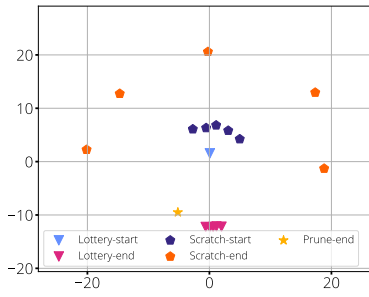
from, but are they in the same basin? Can it be the case that LTs learn significantly different solutions each time in function space despite being linearly connected to the pruning solution?

Lottery Tickets are in the Pruning Solution Basin Investigating paths between different solutions is a popular tool for understanding how various points in parameter space relate to each other in the loss landscape (Goodfellow, Vinyals, and Saxe 2015; Garipov et al. 2018; Draxler et al. 2018; Evci et al. 2019; Fort, Hu, and Lakshminarayanan 2020; Frankle et al. 2020a). For example, Frankle et al. (2019) use linear interpolations to show that LTs always go to the same basin[¶] when trained in different data orders. In Figs. 5c and 5f we look at the linear paths between pruning solution and 4 other points: LT initialization/solution and random (scratch) initialization/solution. Each experiment is repeated 5 times with different random seeds, and mean values are provided with 80% confidence intervals. In both experiments we observe that the linear path between LT initialization and the pruning solution decreases faster compared to the path that originates from scratch initialization. After training, the linear paths towards the pruning solution change drastically. The path from the scratch solution depicts a loss barrier; the scratch solution seems to be in a different basin than the pruning solution[¶]. In contrast, LTs are linearly connected to the pruning solution in both small and large-scale experiments indicating that LTs have the same basin of attraction as the pruning solutions they are derived from. While it seems likely, these results do not however explicitly show that the LT and pruning solutions have learned similar functions.

Lottery Tickets Learn Similar Functions to the Pruning Solution Fort, Hu, and Lakshminarayanan (2020) motivate deep ensembles by empirically showing that models starting from different random initializations typically learn different solutions, as compared to models trained from similar initializations, and thus improve performance. In Appendix F we adopt the analysis of (Fort, Hu, and Lakshminarayanan 2020), but in comparing LT initializations and random initializations using *fractional disagreement* — the fraction of class predictions over which the LT and scratch models disagree with the pruning solution they were derived from, Kullback–Leibler

[¶]We define a basin as a set of points, each of which is linearly connected to at least one other point in the set.

[¶]This is not always true, it is possible that non-linear low energy paths exist between two solutions (Draxler et al. 2018; Garipov et al. 2018), but searching for such paths is outside the scope of this work.

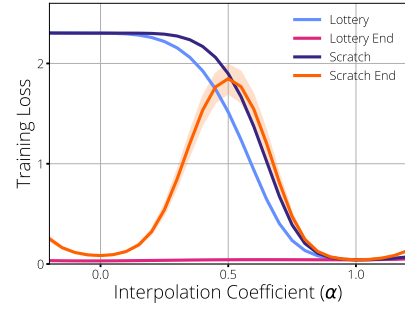


(a) MDS Projection

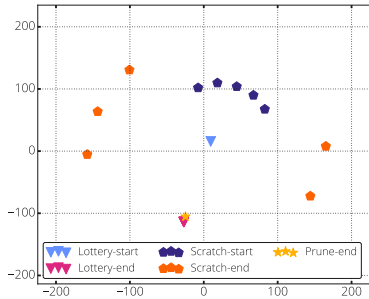
MNIST/LeNet5

Method	LT	Scratch
Acc_{test}	98.52	97.19
d_{init}	13.61	17.46
d_{final}	8.03	25.64

(b) L2 Distances



(c) Loss Interpolation

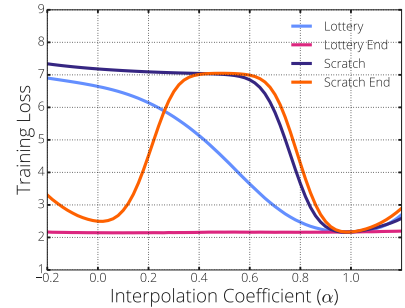


(d) MDS Projection

ImageNet-2012/ResNet-50

Method	LT	Scratch
Acc_{test}	75.74	71.16
d_{init}	147.12	200.44
d_{final}	39.35	215.98

(e) L2 Distances



(f) Loss Interpolation

Figure 5: **MDS Embeddings/L2 Distances**: (a, d): 2D Multi-dimensional Scaling (MDS) embedding of sparse NNs with the same connectivity/mask; (b, e): the average L2-distance between a pruning solution and other derived sparse networks; (c, f): linear path between the pruning solution ($\alpha = 1.0$) and LT/scratch at both initialization, and solution (end of training). Top and bottom rows are for MNIST/LeNet5 and ImageNet-2012/ResNet-50 respectively.

Table 3: **Ensemble & Prediction Disagreement**. We compare the function similarity (Fort, Hu, and Lakshminarayanan 2020) with the original pruning solution and ensemble generalization over 5 sparse models, trained from random initializations and LTs. As a baseline, we also show results for 5 pruned models trained from different random initializations. See Appendix F for full results.

	Initialization	(Top-1) Test Acc.	Ensemble	Disagreement	Disagree. w/ Pruned
LeNet5	LT	98.52±0.02	98.58	0.0043±0.0006	0.0089±0.0002
	Scratch	97.04±0.15	98.00	0.0316±0.0023	0.0278±0.0020
	Scratch (Diff. Init.)	97.19±0.33	98.43	0.0352±0.0037	0.0278±0.0032
	Prune Restart	98.60±0.01	98.63	0.0027±0.0003	0.0077±0.0003
MNIST	Pruned Soln.	98.53	–	–	–
	5 Diff. Pruned	98.30±0.23	99.07	0.0214±0.0023	0.0197±0.0019*
ResNet50	LT	75.73±0.08	76.27	0.0894±0.0009	0.0941±0.0009
	Scratch	71.16±0.13	74.05	0.2039±0.0013	0.2033±0.0012
ImageNet	Pruned Soln.	75.60	–	–	–
	5 Diff. Pruned	75.65±0.13	77.80	0.1620±0.0008	0.1623±0.0011*

* Here we compare 4 different pruned models with the pruning solution LT/Scratch are derived from.

Divergence (KL), and Jensen–Shannon Divergence (JSD). The results in Table 7 suggest LTs models converge on a solution almost identical to the pruning solution and therefore an ensemble of LTs brings marginal improvements. Our results also show that having a fixed initialization alone can not explain the low disagreement observed for LT experiments as *Scratch* solutions obtain an average disagreement of 0.0316 despite using the same initialization, which is almost 10 times larger than that of the LT solutions (0.0043). As a result, LT ensembles show significantly less gains on MNIST and ImageNet-2012 (+0.06% and +0.54% respectively) compared to a random sparse initialization (+0.96% and +2.89%).

Implications: (a) **Rewinding of LTs.** Frankle et al. (2019, 2020a) argued that LTs work when the training is *stable*, and thus converges to the same basin when trained with different data sampling orders. In §4.3, we show that this basin is the same one found by pruning, and since the training converges to the same basin as before, we expect to see limited gains from rewinding if any. This is partially confirmed by Renda, Frankle, and Carbin (2020) which shows that restarting the learning rate schedule from the pruning solution performs better than rewinding the weights. (b) **Transfer of LTs.** Given the close relationship between LTs and pruning solutions, the observation that LTs trained on large datasets transfer to smaller ones, but not *vice versa* (Morcos et al. 2019; Sabatelli, Kestemont, and Geurts 2020) can be explained by a common observation in transfer learning: networks trained in large datasets transfer to smaller ones. (c) **LT’s Robustness to Perturbations.** Zhou et al. (2019); Frankle, Schwab, and Morcos (2020) found that certain perturbations, like only using the signs of weights at initialization, do not impact LT generalization, while others, like shuffling the weights, do. Our results bring further insights to these observations: As long as the perturbation is small enough such that a LT stays in the same basin of attraction, results will be as good as the pruning solution. (d) **Success of LTs.** While it is exciting to see widespread applicability of LTs in different domains (Brix, Bahar, and Ney 2020; Li et al. 2020; Venkatesh et al. 2020), the results presented in this paper suggest this success may be due to the underlying pruning algorithm (and transfer learning) rather than LT initializations themselves.

5 Conclusion

In this work we studied (1) why training unstructured sparse networks from random initialization performs poorly and; (2) what makes LTs and DST the exceptions? We identified that randomly initialized unstructured sparse NNs exhibit poor gradient flow when initialized naively and proposed an alternative initialization that scales the initial variance for each neuron separately. Furthermore we showed that modern sparse NN architectures are more sensitive to poor gradient flow during early training rather than initialization alone. We observed that this is somewhat addressed by state-of-the-art DST methods, such as RigL, which significantly improves gradient flow during early training over traditional sparse training methods. Finally, we show that LTs do not improve gradient flow at either initialization or during training, but

rather their success lies in effectively re-learning the original pruning solution they are derived from. We showed that a LTs initialization resides within the same basin of attraction as the pruning solution and, furthermore, when trained the LT solution learns a highly similar solution to the pruning solution, limiting their ensemble performance. These findings suggest that LTs are fundamentally limited in their potential for improving the training of sparse NNs more generally.

Acknowledgements

We like to thank members of the Google Brain team for their useful feedback and support. Specifically, we thank Sara Hooker, Fabian Pedregosa, Laura Graesser, Ilya Tolstikhin, Erich Elsen, Ross Goroshin and Danny Tarlow for providing feedback on the preprint. We thank Ying Xiao for helping out calculating hessian of large networks.

References

- Brix, C.; Bahar, P.; and Ney, H. 2020. Successfully Applying the Stabilized Lottery Ticket Hypothesis to the Transformer Architecture. *ArXiv*.
- Chen, T.; Cheng, Y.; Gan, Z.; Yuan, L.; Zhang, L.; and Wang, Z. 2021. Chasing Sparsity in Vision Transformers: An End-to-End Exploration. *ArXiv*, abs/2106.04533.
- Curci, S.; Mocanu, D. C.; and Pechenizkiy, M. 2021. Truly Sparse Neural Networks at Scale. *ArXiv*.
- Dettmers, T.; and Zettlemoyer, L. 2019. Sparse Networks from Scratch: Faster Training without Losing Performance. *ArXiv*.
- Dietrich, A.; Gressmann, F.; Orr, D.; Chelombiev, I.; Justus, D.; and Luschi, C. 2021. Towards Structured Dynamic Sparse Pre-Training of BERT. *ArXiv*.
- Draxler, F.; Veschgini, K.; Salmhofer, M.; and Hamprecht, F. A. 2018. Essentially No Barriers in Neural Network Energy Landscape. In *International Conference on Machine Learning*.
- Evci, U.; Gale, T.; Menick, J.; Castro, P. S.; and Elsen, E. 2020. Rigging the Lottery: Making All Tickets Winners. In *Proceedings of Machine Learning and Systems 2020*, 471–481. PMLR.
- Evci, U.; Pedregosa, F.; Gomez, A. N.; and Elsen, E. 2019. The Difficulty of Training Sparse Neural Networks. *ArXiv*.
- Fort, S.; Hu, H.; and Lakshminarayanan, B. 2020. Deep Ensembles: A Loss Landscape Perspective. In *International Conference on Learning Representations*.
- Frankle, J.; and Carbin, M. 2019. The Lottery Ticket Hypothesis: Finding Sparse, Trainable Neural Networks. In *7th International Conference on Learning Representations (ICLR)*.
- Frankle, J.; Dziugaite, G. K.; Roy, D. M.; and Carbin, M. 2019. Stabilizing the Lottery Ticket Hypothesis. *ArXiv*.
- Frankle, J.; Dziugaite, G. K.; Roy, D. M.; and Carbin, M. 2020a. Linear Mode Connectivity and the Lottery Ticket Hypothesis. In *Proceedings of the International Conference on Machine Learning*.

- Frankle, J.; Dziugaite, G. K.; Roy, D. M.; and Carbin, M. 2020b. Pruning Neural Networks at Initialization: Why are We Missing the Mark? *ArXiv*.
- Frankle, J.; Schwab, D. J.; and Morcos, A. S. 2020. The Early Phase of Neural Network Training. In *International Conference on Learning Representations*.
- Gale, T.; Elsen, E.; and Hooker, S. 2019. The State of Sparsity in Deep Neural Networks. *ArXiv*.
- Garipov, T.; Izmailov, P.; Podoprikin, D.; Vetrov, D. P.; and Wilson, A. G. 2018. Loss Surfaces, M Connectivity, and Fast Ensembling of DNNs. In *Advances in Neural Information Processing Systems*.
- Ghorbani, B.; Krishnan, S.; and Xiao, Y. 2019. An Investigation into Neural Net Optimization via Hessian Eigenvalue Density. In *Proceedings of the 36th International Conference on Machine Learning*.
- Glorot, X.; and Bengio, Y. 2010. Understanding the difficulty of training deep feedforward neural networks. In *Proceedings of the 13th International Conference on Artificial Intelligence and Statistics (AISTATS)*.
- Golubeva, A.; Neyshabur, B.; and Gur-Ari, G. 2021. Are wider nets better given the same number of parameters? *ArXiv*, abs/2010.14495.
- Goodfellow, I. J.; Vinyals, O.; and Saxe, A. M. 2015. Qualitatively characterizing neural network optimization problems. In *International Conference on Learning Representations*.
- Han, S.; Pool, J.; Tran, J.; and Dally, W. 2015. Learning both weights and connections for efficient neural network. In *Advances in neural information processing systems*.
- He, K.; Zhang, X.; Ren, S.; and Sun, J. 2015. Delving Deep into Rectifiers: Surpassing Human-Level Performance on ImageNet Classification. In *IEEE International Conference on Computer Vision (ICCV)*.
- Ioffe, S.; and Szegedy, C. 2015. Batch Normalization: Accelerating Deep Network Training by Reducing Internal Covariate Shift. In *Proceedings of the 32Nd International Conference on International Conference on Machine Learning*.
- Kruskal, J. 1964. Multidimensional scaling by optimizing goodness of fit to a nonmetric hypothesis. *Psychometrika*.
- Kusupati, A.; Ramanujan, V.; Somani, R.; Wortsman, M.; Jain, P.; Kakade, S.; and Farhadi, A. 2020. Soft Threshold Weight Reparameterization for Learnable Sparsity. In *Proceedings of the International Conference on Machine Learning*.
- LeCun, Y.; Boser, B.; Denker, J. S.; Henderson, D.; Howard, R. E.; Hubbard, W.; and Jackel, L. D. 1989. Backpropagation applied to handwritten zip code recognition. *Neural Computation*.
- Lee, N.; Ajanthan, T.; Gould, S.; and Torr, P. H. S. 2020. A Signal Propagation Perspective for Pruning Neural Networks at Initialization. In *ICLR*.
- Lee, N.; Ajanthan, T.; and Torr, P. H. S. 2019. SNIP: Single-shot Network Pruning based on Connection Sensitivity. In *ICLR*.
- Lewkowycz, A.; Bahri, Y.; Dyer, E.; Sohl-Dickstein, J.; and Gur-Ari, G. 2020. The large learning rate phase of deep learning: the catapult mechanism. *Arxiv*.
- Li, B.; Wang, S.; Jia, Y.; Lu, Y.; Zhong, Z.; Carin, L.; and Jana, S. 2020. Towards Practical Lottery Ticket Hypothesis for Adversarial Training. *ArXiv*.
- Liu, S.; Chen, T.; Atashgahi, Z.; Chen, X.; Sokar, G.; Mocanu, E.; Pechenizkiy, M.; Wang, Z.; and Mocanu, D. C. 2021a. FreeTickets: Accurate, Robust and Efficient Deep Ensemble by Training with Dynamic Sparsity. *ArXiv*.
- Liu, S.; Ni'mah, I.; Menkovski, V.; Mocanu, D.; and Pechenizkiy, M. 2021b. Efficient and effective training of sparse recurrent neural networks. *Neural Comput. Appl.*, 33: 9625–9636.
- Liu, S.; Yin, L.; Mocanu, D.; and Pechenizkiy, M. 2021c. Do We Actually Need Dense Over-Parameterization? In-Time Over-Parameterization in Sparse Training. In *ICML*.
- Liu, Z.; Sun, M.; Zhou, T.; Huang, G.; and Darrell, T. 2019. Rethinking the Value of Network Pruning. In *International Conference on Learning Representations*.
- Louizos, C.; Ullrich, K.; and Welling, M. 2017. Bayesian compression for deep learning. In *Advances in Neural Information Processing Systems*.
- Lubana, E. S.; and Dick, R. 2021. A Gradient Flow Framework For Analyzing Network Pruning. In *International Conference on Learning Representations (ICLR), 2021*.
- Maene, J.; Li, M.; and Moens, M. 2021. Towards Understanding Iterative Magnitude Pruning: Why Lottery Tickets Win. *ArXiv*.
- Mocanu, D. C.; Mocanu, E.; Stone, P.; Nguyen, P. H.; Gibescu, M.; and Liotta, A. 2018. Scalable training of artificial neural networks with adaptive sparse connectivity inspired by network science. *Nature Communications*.
- Molchanov, D.; Ashukha, A.; and Vetrov, D. 2017. Variational Dropout Sparsifies Deep Neural Networks. In *Proceedings of the 34th International Conference on Machine Learning*, Proceedings of Machine Learning Research. International Convention Centre, Sydney, Australia: PMLR.
- Morcos, A.; Yu, H.; Paganini, M.; and Tian, Y. 2019. One ticket to win them all: generalizing lottery ticket initializations across datasets and optimizers. In *Advances in Neural Information Processing Systems 32*.
- Mostafa, H.; and Wang, X. 2019. Parameter efficient training of deep convolutional neural networks by dynamic sparse reparameterization. In *Proceedings of the 36th International Conference on Machine Learning, ICML 2019, 9-15 June 2019, Long Beach, California, USA*.
- Mozer, M. C.; and Smolensky, P. 1989. Skeletonization: A Technique for Trimming the Fat from a Network via Relevance Assessment. In *Advances in Neural Information Processing Systems I*. Morgan-Kaufmann.
- Papayan, V. 2019. Measurements of Three-Level Hierarchical Structure in the Outliers in the Spectrum of Deepnet Hessians. *ArXiv*.

Price, I.; and Tanner, J. 2021. Dense for the Price of Sparse: Improved Performance of Sparsely Initialized Networks via a Subspace Offset. *ArXiv*, abs/2102.07655.

Ramanujan, V.; Wortsman, M.; Kembhavi, A.; Farhadi, A.; and Rastegari, M. 2019. What’s Hidden in a Randomly Weighted Neural Network? *ArXiv*.

Renda, A.; Frankle, J.; and Carbin, M. 2020. Comparing Rewinding and Fine-tuning in Neural Network Pruning. In *International Conference on Learning Representations*.

Russakovsky, O.; Deng, J.; Su, H.; Krause, J.; Satheesh, S.; Ma, S.; Huang, Z.; Karpathy, A.; Khosla, A.; Bernstein, M.; Berg, A. C.; and Fei-Fei, L. 2015. ImageNet Large Scale Visual Recognition Challenge. *International Journal of Computer Vision (IJCV)*.

Sabatelli, M.; Kestemont, M.; and Geurts, P. 2020. On the Transferability of Winning Tickets in Non-Natural Image Datasets. *ArXiv*.

Sagun, L.; Evci, U.; Güney, V. U.; Dauphin, Y.; and Bottou, L. 2017. Empirical Analysis of the Hessian of Over-Parametrized Neural Networks. In *International Conference on Learning Representations*.

Sokar, G.; Mocanu, E.; Mocanu, D. C.; Pechenizkiy, M.; and Stone, P. 2021. Dynamic Sparse Training for Deep Reinforcement Learning. *ArXiv*.

Tanaka, H.; Kunin, D.; Yamins, D. L. K.; and Ganguli, S. 2020. Pruning neural networks without any data by iteratively conserving synaptic flow. In *Advances in Neural Information Processing Systems*.

Tessera, K.; Hooker, S.; and Rosman, B. 2021. Keep the Gradients Flowing: Using Gradient Flow to Study Sparse Network Optimization. *ArXiv*.

van der Walt, S.; Colbert, S. C.; and Varoquaux, G. 2011. The NumPy Array: A Structure for Efficient Numerical Computation. *Computing in Science Engineering*.

Venkatesh, B.; Thiagarajan, J. J.; Thopalli, K.; and Sattigeri, P. 2020. Calibrate and Prune: Improving Reliability of Lottery Tickets Through Prediction Calibration. *ArXiv*.

Wang, C.; Zhang, G.; and Grosse, R. 2020. Picking Winning Tickets Before Training by Preserving Gradient Flow. In *ICLR*.

Wu, S.; Zhong, S.; and Liu, Y. 2018. Deep residual learning for image steganalysis. *Multimedia Tools and Applications*.

Xiao, L.; Bahri, Y.; Sohl-Dickstein, J.; Schoenholz, S. S.; and Pennington, J. 2018. Dynamical isometry and a mean field theory of cnns: How to train 10,000-layer vanilla convolutional neural networks. In *International Conference on Machine Learning (ICML)*.

Zhang, H.; Dauphin, Y. N.; and Ma, T. 2019. Fixup Initialization: Residual Learning Without Normalization. In *International Conference on Learning Representations*.

Zhou, H.; Lan, J.; Liu, R.; and Yosinski, J. 2019. Deconstructing lottery tickets: Zeros, signs, and the supermask. In *Advances in Neural Information Processing Systems*.

Zhu, M.; and Gupta, S. 2018. To Prune, or Not to Prune: Exploring the Efficacy of Pruning for Model Compression. In *International Conference on Learning Representations Workshop*.

A Experimental Details

A.1 Details of Experiments in Section 4.3

The training hyper-parameters used in §4.3 are shared in Table 4. All experiments in this section start with a pruning experiment, after which the sparsity masks found by pruning are used to perform LT experiments. We use iterative magnitude pruning (Zhu and Gupta 2018) in our experiments, which is a well studied and more efficient pruning method as compared to the one used by Frankle and Carbin (2019). Our pruning algorithm performs iterative pruning without rewinding the weights between intermediate steps and requires significantly less iterations. We expect our results would be even more pronounced with additional rewinding steps.

We use SGD with momentum in all of our experiments. *Scratch* and *Lottery* experiments use the same hyper-parameters. Additional specific details of our experiments are shared below.

LeNet5 We prune all layers of LeNet5, so that they reach 95% final sparsity (i.e. 95% of the parameters are zeros). We choose this sparsity, since at this sparsity, we start observing stark differences between *Lottery* and *Scratch* in terms of performance. We set the weight decay to zero, similar to the MNIST experiments done in the original LT paper (Frankle and Carbin 2019) and do a grid search over learning-rates={0.1,0.2,0.05,0.02,0.01}. Loss values for the linear interpolation experiments are calculated on the entire training set.

ResNet50 We prune all layers of ResNet50, except the first layer, so that they reach 80% final sparsity. In this setting rewinding to the original initialization doesn’t work, hence we use values from 6th epoch. Loss values for the linear interpolation experiments are calculated using 500,000 images from the ImageNet-2012 training set.

A.2 Details of Experiments in Section 4.1 and 4.2

Training hyper-parameters used for these experiments are shared in Table 5.

MNIST In this setting, the hyper-parameters are almost same as in §4.3, except we enable weight decay as it brings better generalization. We do a grid search over weight-decays={0.001,0.0001,0.00005,0.00001,0.0005} and learning-rates={0.1,0.2,0.05,0.02,0.01} and pick the values with top test accuracy. We use the masks found by pruning experiments in all of our MNIST experiments in this section to isolate the effect of the initialization. We simplify the update schedule of Dynamic Sparse Training (DST) methods such that they decay with learning rate. This approach fits well, since the original decay function used in these experiments is the cosine decay which is the same as our learning rate schedule. We scale learning rate such that it matches the initial drop fraction provided. Mask update frequency and initial drop fraction are chosen from a grid search of {50, 100, 500} and {0.01,0.1,0.3} respectively. To allow fair comparison, we use Glorot scaling in all of our initializations (i.e. scale=1 and we average fan-in fan-out values) as it is the default initialization for Tensorflow layers and our results shows that it out-performs He initialization by a small margin with the

Table 4: **§4.3: Experiment Details/Hyperparameters.** Initial Learning Rate (LR), LR Schedule (Sched.), Batchsize (Batch.), Momentum (m), Weight Decay (WD), t_{start} , t_{end} and f are the pruning starting iteration, end iteration, and mask update frequency respectively.

Dataset	Model	t_{total}	Epochs	Batch.	LR	Sched.	m	WD	Sparsity	Pruning		
										t_{start}	t_{end}	f
MNIST	LeNet5	11719	30	128	0.05	Cosine	0.9	0	95%	3000	7000	100
ImageNet	ResNet50	32000	≈ 102	4096	1.6	Step*	0.9	1×10^{-4}	80%	5000	8000	2000

* Step schedule has a linear warm-up in first 5 epochs and decreases the learning rate by a factor of 10 at epochs 30, 70 and 90.

Table 5: **§4.1: Experiment Details/Hyperparameters.** Initial Learning Rate (LR), LR Schedule (Sched.), Batchsize (Batch.), Momentum (m), Weight Decay (WD), Initial Drop Fraction (Drop.), t_{end} and f are the pruning mask update frequency and end iteration respectively. *LeNet5+* row corresponds the LeNet5 experiments with our sparse initialization, whereas *LeNet5* is the regular masked initialization.

Dataset	Model	t_{total}	Epochs	Batch.	LR	Sched.	m	WD	Sparsity	DST		
										Drop.	f	t_{end}
MNIST	LeNet5	11719	30	128	0.05	Cosine	0.9	5×10^{-4}	95%	0.3	500	11719
ImageNet	ResNet50	32000	≈ 102	4096	1.6	Step*	0.9	1×10^{-4}	80%	0.3	100	25000
	VGG16	128000		1024	0.04					0.1	500	

* Step schedule has a linear warm-up in first 5 epochs and decreases the learning rate by a factor of 10 at epochs 30, 70 and 90.

hyper-parameters used. Using He initialization brings similar results.

Hessian calculation The Hessian is calculated on full training set using Hessian-vector products. We mask our network after each gradient call and calculate only non-zero rows. After calculating the full Hessian, we use `numpy.eigh` (van der Walt, Colbert, and Varoquaux 2011) to calculate eigenvalues of the Hessian.

ImageNet-2012 In this setting, hyper-parameters are almost the same as in §4.3 except for VGG16 architecture, where we use a smaller batch size and learning rate. For all DST methods, we use a cosine drop schedule (Dettmers and Zettlemoyer 2019) and hyper-parameters proposed by Evci et al. (2019). For VGG, we reduce the mask update frequency and the initial drop fraction, as we observe better performance after doing a grid search over $\{50, 100, 500\}$ and $\{0.1, 0.3, 0.5\}$ respectively. We also use a non-uniform (ERK) sparsity distribution among layers as described in Evci et al. (2020), since we observed that it brings better performance.

B Glorot/He Initialization Generalized to Neural Networks with Heterogeneous Connectivity: Full Explanation/Derivation

Here we derive the full generalized initialization for both the forwards/backwards cases (i.e. fan-in/fan-out), refer to Fig. 6 for an illustration of how the connectivity for the fan-in/fan-out cases are determined for each neuron.

B.1 Generalized Glorot/He Initialization: Backwards, Forwards and Average Cases

For every weight $w_{ij}^{[\ell]} \in W^{n^{[\ell]} \times n^{[\ell-1]}}$ in a layer ℓ with $n^{[\ell]}$ neurons, connecting neuron i in layer ℓ to neuron j in layer $(\ell - 1)$ with $n^{[\ell-1]}$ neurons, and weight mask $[m_{ij}^{[\ell]}] = M^\ell \in [0, 1]^{n^{[\ell]} \times n^{[\ell-1]}}$,

$$\begin{aligned} \text{Glorot and Bengio (2010): } & w_{ij}^{[\ell]} \sim \mathcal{N}\left(0, \frac{1}{u}\right) \\ \text{He et al. (2015): } & w_{ij}^{[\ell]} \sim \mathcal{N}\left(0, \frac{2}{u}\right) \end{aligned} \quad (2)$$

$$u = \begin{cases} \text{fan-in}_i^{[\ell]} & \text{(forward)} \\ \text{fan-out}_j^{[\ell]} & \text{(backward)} \\ (\text{fan-in}_i^{[\ell]} + \text{fan-out}_j^{[\ell]}) / 2 & \text{(average)} \end{cases}$$

where,

$$\text{fan-in}_i^{[\ell]} = \sum_{j=1}^{n^{[\ell-1]}} m_{ij}^{[\ell]}, \quad \text{fan-out}_j^{[\ell]} = \sum_{i=1}^{n^{[\ell]}} m_{ij}^{[\ell]},$$

are the number of incoming and outgoing connections respectively. In the special case of a dense layer where $m_{ij}^{[\ell]} = 1, \forall i, j$, Eq. (1) reduces to the initializations proposed by (Glorot and Bengio 2010; He et al. 2015) since $\text{fan-in}_i^{[\ell]} = n^{[\ell-1]}, \forall i$, and $\text{fan-out}_j^{[\ell]} = n^{[\ell]}, \forall j$.

B.2 Derivation: Fixed Mask, Forward Propagation

Given a sparse NN, where the output of a neuron a_i is given by, $a_i^{[\ell]} = f(z_i^{[\ell]})$, where $z_i^{[\ell]} = \sum_j^{n^{[\ell-1]}} m_{ij}^{[\ell]} w_{ij}^{[\ell]} a_j^{[\ell-1]}$,

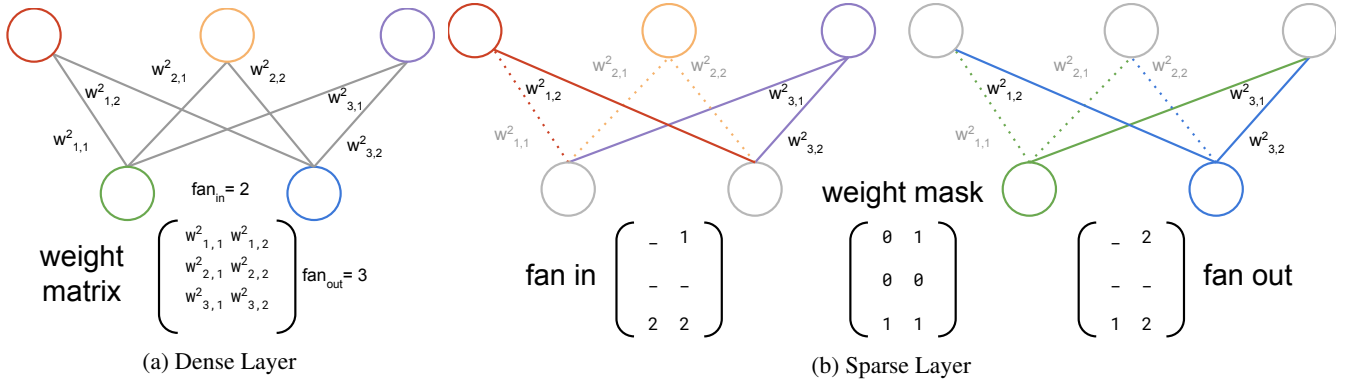


Figure 6: **Glorot/He Initialization for a Sparse NN.** (Glorot and Bengio 2010; He et al. 2015) restrict the outputs of all neurons to be zero-mean and of unit variance. All neurons in a dense NN layer (a) have the same fan-in/fan-out, whereas in a sparse NN (b) the fan-in/fan-out can differ for *every neuron*, potentially requiring sampling from a different distribution for every neuron. The fan-in matrix contains the values used in Eq. (1) for each neuron.

where $m_{ij}^{[\ell]} \in M^{[\ell]}$ and $w_{ij}^{[\ell]} \in W^{[\ell]}$ are the mask and weights respectively for layer ℓ , and $a_j^{[\ell-1]}$ the output of the previous layer. Assume the mask $M^{[\ell]} \in \mathbb{1}^{n^{[\ell]} \times n^{[\ell-1]}}$ is constant, where $\mathbb{1}^{n^{[\ell]} \times n^{[\ell-1]}}$ is an indicator matrix.

As in Glorot and Bengio (2010) we want to ensure $\text{Var}(a_i^{[\ell]}) = \text{Var}(a_i^{[\ell-1]})$, and $\text{mean}(a_i^{[\ell]}) = 0$. Assume that $f(x) \approx x$ for x close to 0, e.g. in the case of $f(x) = \tanh(x)$, and that $w_{ij}^{[\ell]}$ and $a_j^{[\ell-1]}$ are independent,

$$\text{Var}(a_i^{[\ell-1]}) \approx \text{Var}(z_i^{[\ell]}) \quad (3)$$

$$= \text{Var} \left(\sum_{j=1}^{n^{[\ell-1]}} m_{ij}^{[\ell]} w_{ij}^{[\ell]} a_j^{[\ell-1]} \right) \quad (4)$$

$$= \sum_{j=1}^{n^{[\ell-1]}} \text{Var} \left(m_{ij}^{[\ell]} w_{ij}^{[\ell]} a_j^{[\ell-1]} \right) \quad (5)$$

$$\text{(independent sum)} \quad (6)$$

$$= \sum_{j=1}^{n^{[\ell-1]}} \left(m_{ij}^{[\ell]} \right)^2 \text{Var} \left(w_{ij}^{[\ell]} a_j^{[\ell-1]} \right) \quad (7)$$

$$\because m_{ij}^{[\ell]} \text{ is constant, } \text{Var}(cX) = c^2 \text{Var}(X) \quad (8)$$

$$= \sum_{j=1}^{n^{[\ell-1]}} m_{ij}^{[\ell]} \text{Var} \left(w_{ij}^{[\ell]} a_j^{[\ell-1]} \right) \quad (9)$$

$$\because m_{ij}^{[\ell]} \in [0, 1], \left(m_{ij}^{[\ell]} \right)^2 = m_{ij}^{[\ell]}. \quad (10)$$

$$= \sum_{j=1}^{n^{[\ell-1]}} m_{ij}^{[\ell]} \text{Var}(w_{ij}^{[\ell]}) \text{Var}(a_j^{[\ell-1]}). \quad (11)$$

$$\text{(independent product)} \quad (12)$$

Assume $\text{Var}(w_{im}^{[\ell]}) = \text{Var}(w_{in}^{[\ell]})$, $\forall n, m$, i.e. the variance

of all weights for a given neuron are the same, and $\text{Var}(a_n^{[\ell-1]}) = \text{Var}(a_m^{[\ell-1]})$, i.e. the variance of any of the outputs of the previous layer are the same. Therefore we can simplify Eq. (12),

$$\text{Var}(a_i^{[\ell-1]}) = \sum_{j=1}^{n^{[\ell-1]}} m_{ij}^{[\ell]} \text{Var}(w_{ij}^{[\ell]}) \text{Var}(a_j^{[\ell-1]}) \quad (13)$$

$$= \text{Var}(w_{ij}^{[\ell]}) \text{Var}(a_j^{[\ell-1]}) \sum_{j=1}^{n^{[\ell-1]}} m_{ij}^{[\ell]}. \quad (14)$$

Let neuron i 's number of non-masked weights be denoted $\text{fan-in}_i^{[\ell]}$, where $\text{fan-in}_i^{[\ell]} = \sum_{j=1}^{n^{[\ell-1]}} m_{ij}^{[\ell]}$, then

$$\text{Var}(a_i^{[\ell-1]}) = \text{fan-in}_i^{[\ell]} \text{Var}(w_{ij}^{[\ell]}) \text{Var}(a_j^{[\ell-1]}) \quad (15)$$

$$\text{Recall, } \text{Var}(a_i^{[\ell-1]}) = \text{Var}(a_j^{[\ell-1]})$$

$$\Rightarrow \text{Var}(w_{ij}^{[\ell]}) = \frac{1}{\text{fan-in}_i^{[\ell]}}. \quad (16)$$

Therefore, in order to have the output of each neuron $a_i^{[\ell]}$ in layer ℓ to have unit variance, and mean 0, we need to sample the weights for each neuron from the normal distribution,

$$[w_{ij}^{[\ell]}] \sim \mathcal{N} \left(0, \frac{1}{\text{fan-in}_i^{[\ell]}} \right), \quad (17)$$

where s_i^ℓ is the sparsity of weights of the neuron with output a_i . For the ReLU activation function, following the derivation in He et al. (2015),

$$[w_{ij}^{[\ell]}] \sim \mathcal{N} \left(0, \frac{2}{\text{fan-in}_i^{[\ell]}} \right). \quad (18)$$

B.3 Fixed Mask: Backward Pass

Given a sparse NN, where the output of a neuron a_i is given by, $a_i^{[\ell]} = f(z_i^{[\ell]})$, where $z_i^{[\ell]} = \sum_{j=1}^{n^{[\ell-1]}} m_{ij}^{[\ell]} w_{ij}^{[\ell]} a_j^{[\ell-1]}$,

where $m_{ij}^{[\ell]} \in M^{[\ell]}$ and $w_{ij}^{[\ell]} \in W^{[\ell]}$ are the mask and weights respectively for layer ℓ , and $a_j^{[\ell-1]}$ the output of the previous layer. Assume the mask $M^{[\ell]} \in \mathbb{1}^{n^{[\ell]} \times n^{[\ell-1]}}$ is constant, where $\mathbb{1}^{n^{[\ell]} \times n^{[\ell-1]}}$ is an indicator matrix, and let $L(\theta = \{W^{[\ell]}, \ell = 0 \dots N\})$ be the loss we are optimizing.

As in Glorot and Bengio (2010), from the backward-propagation standpoint, we want to ensure $\text{Var}(\frac{\partial L}{\partial z_i^{[\ell]}}) = \text{Var}(\frac{\partial L}{\partial z_i^{[\ell-1]}})$, and $\text{mean}(\frac{\partial L}{\partial z_i^{[\ell]}}) = 0$. Assume that $f'(0) = 1$,

$$\text{Var}(\frac{\partial L}{\partial z_j^{[\ell]}}) \approx \text{Var}(\frac{\partial L}{\partial a_j^{[\ell-1]}}) \quad (19)$$

$$= \text{Var}\left(\sum_{i=1}^{n^{[\ell]}} m_{ij}^{[\ell]} w_{ij}^{[\ell]} \frac{\partial L}{\partial z_i^{[\ell]}}\right) \quad (20)$$

$$= \sum_{i=1}^{n^{[\ell]}} \text{Var}\left(m_{ij}^{[\ell]} w_{ij}^{[\ell]} \frac{\partial L}{\partial z_i^{[\ell]}}\right) \quad (21)$$

(independent sum)

$$= \sum_{i=1}^{n^{[\ell]}} (m_{ij}^{[\ell]})^2 \text{Var}\left(w_{ij}^{[\ell]} \frac{\partial L}{\partial z_i^{[\ell]}}\right) \quad (22)$$

$\because m_{ij}^{[\ell]}$ is constant, $\text{Var}(cX) = c^2 \text{Var}(X)$

$$= \sum_{i=1}^{n^{[\ell]}} m_{ij}^{[\ell]} \text{Var}\left(w_{ij}^{[\ell]} \frac{\partial L}{\partial z_i^{[\ell]}}\right) \quad (23)$$

$\because m_{ij}^{[\ell]} \in [0, 1], (m_{ij}^{[\ell]})^2 = m_{ij}^{[\ell]}$.

$$= \sum_{i=1}^{n^{[\ell]}} m_{ij}^{[\ell]} \text{Var}(w_{ij}^{[\ell]}) \text{Var}\left(\frac{\partial L}{\partial z_i^{[\ell]}}\right). \quad (24)$$

(independent product)

Assume $\text{Var}(w_{mj}^{[\ell]}) = \text{Var}(w_{nj}^{[\ell]})$, $\forall n, m$, i.e. the variance of all weights for a given neuron are the same, and $\text{Var}(\frac{\partial L}{\partial z_n^{[\ell]}}) = \text{Var}(\frac{\partial L}{\partial z_m^{[\ell]}})$, i.e. the variance of the output gradients of each neuron at layer l are the same. Then we can simplify Eq. (25),

$$\text{Var}(\frac{\partial L}{\partial z_j^{[\ell]}}) = \sum_{i=1}^{n^{[\ell]}} m_{ij}^{[\ell]} \text{Var}(w_{ij}^{[\ell]}) \text{Var}\left(\frac{\partial L}{\partial z_i^{[\ell]}}\right) \quad (25)$$

$$= \text{Var}(w_{ij}^{[\ell]}) \text{Var}\left(\frac{\partial L}{\partial z_i^{[\ell]}}\right) \sum_{i=1}^{n^{[\ell]}} m_{ij}^{[\ell]}. \quad (26)$$

Let neuron i 's number of non-masked weights be denoted

$\text{fan-out}_j^{[\ell]}$, where $\text{fan-out}_j^{[\ell]} = \sum_{i=1}^{n^{[\ell]}} m_{ij}^{[\ell]}$, then

$$\text{Var}(\frac{\partial L}{\partial z_j^{[\ell]}}) = \text{fan-out}_j^{[\ell]} \text{Var}(w_{ij}^{[\ell]}) \text{Var}\left(\frac{\partial L}{\partial z_i^{[\ell]}}\right) \quad (27)$$

$$\text{Recall, } \text{Var}(\frac{\partial L}{\partial z_j^{[\ell]}}) = \text{Var}\left(\frac{\partial L}{\partial z_i^{[\ell]}}\right)$$

$$\Rightarrow \text{Var}(w_{ij}^{[\ell]}) = \frac{1}{\text{fan-out}_j^{[\ell]}}. \quad (28)$$

Therefore, in order to have the output of each neuron $a_i^{[\ell]}$ in layer ℓ to have unit variance, and mean 0, we need to sample the weights for each neuron from the normal distribution,

$$[w_{ij}^{[\ell]}] \sim \mathcal{N}\left(0, \frac{1}{\text{fan-in}_i^{[\ell]}}\right), \quad (29)$$

where s_i^ℓ is the sparsity of weights of the neuron with output a_i . For the ReLU activation function, following the derivation in He et al. (2015),

$$[w_{ij}^{[\ell]}] \sim \mathcal{N}\left(0, \frac{2}{\text{fan-in}_i^{[\ell]}}\right). \quad (30)$$

C Additional Gradient Flow Plots

Here we share additional gradient flow figures for method/initialization combinations presented in 3 and 2.

In Fig. 7b, we show the gradient flow for DST methods and scratch training. Using RigL helps improve gradient flow with both initialization; helping learning to start earlier than regular *Scratch* training. SET seem to have limited effect on the gradient flow.

In Fig. 7b, we share gradient flow when the scaled initialization of (Liu et al. 2019) is used. Similar to the proposed initialization, we observe improved gradient flow for all cases. Different than our initialization however, RigL doesn't improve gradient flow in this setting; highlighting an interesting future research direction on the relationship between initialization and the DST methods.

In Fig. 7c, we share gradient flow when He initialization is used instead of Glorot initialization. We observe that *Scratch* training starts learning faster in this case. Gradient flow seems to be similar for other sparse initialization methods.

In Fig. 8, we share gradient flow improvements after DST updates on connectivity for different initialization methods. ResNet-50 curves match the results in Fig. 3. LeNet5 curves however seem to be adversely affected by poor initialization at the beginning of the training. We start observing improvements with RigL when the learning starts (around the 400th iteration).

D Fully Connected Neural Network Experiments on MNIST

In this section we repeat our experiments from §4.1 using different sparse initialization methods, and analyzing gradient flow, for a standard 2-layer fully-connected NN with 2 hidden layers of size 300 and 100 units. We use the same grid used

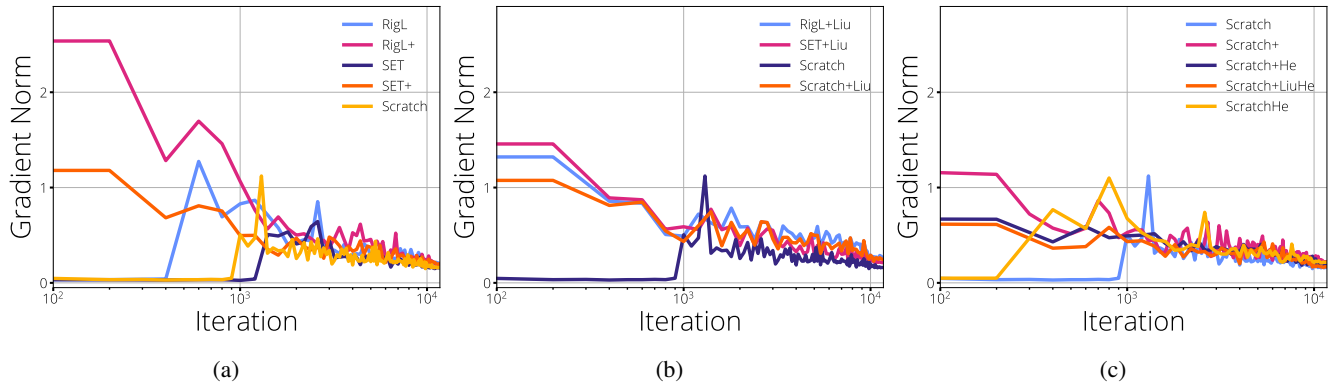


Figure 7: **Gradient Flow of Sparse LeNet-5s during Training.** Gradient flow during training averaged over multiple runs, ‘+’ indicates training runs with our proposed sparse initialization. ‘+Liu’ indicates initialization proposed by (Liu et al. 2019). ‘He’ suffix refers to He initialization where ‘scale=2’ and ‘fanin’ options are used for the variance scaling initialization.

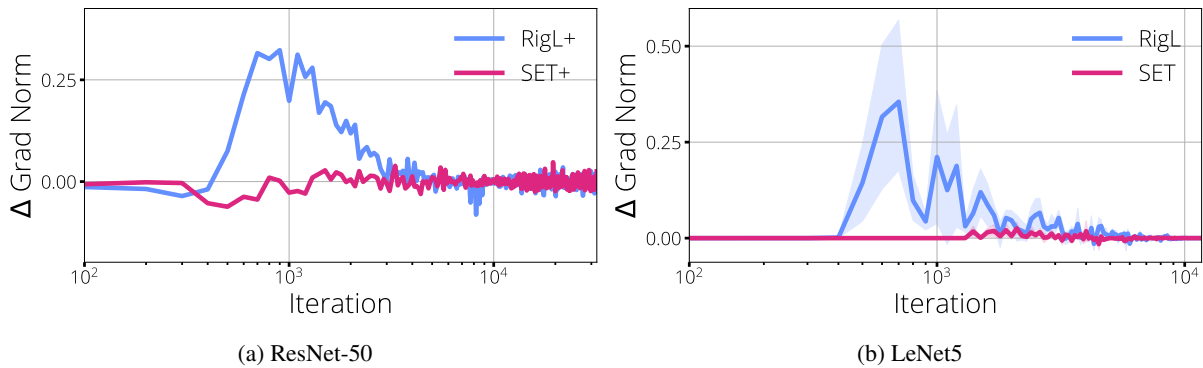


Figure 8: **Effect of Mask Updates in Dynamic Sparse Training.** Effect of mask updates on the gradient norm. We measure the gradient norm before and after the mask updates and plot the Δ . ‘+’ indicates proposed initialization and used in MNIST experiments.

Table 6: **Results of Trained Fully-Connected MNIST Model from Different Initializations.**

	MNIST		
	Fully-Connected NN (98% sparse)		
Baseline	98.55±0.04		
Lottery	97.73±0.11		
Small Dense	91.69±1.85		
	Original	Liu et al.	Ours
Scratch	94.40±4.00	96.66±0.18	96.70±0.12
SET	96.49±0.36	96.56±0.22	96.48±0.10
RigL	96.82±0.25	96.76±0.19	96.94±0.12

in LeNet5 experiments for hyper-parameter selection. Best results were obtained with a learning rate of 0.2, a weight decay coefficient of 0.0001 and an mask update frequency of 500 (used in DST methods). The rest of the hyperparameters remained unchanged from the LeNet5 experiments.

The results of training with various initialization methods is shown in Table 6. Although the results are not as drastic as with LeNet5, we see that here too sparsity aware initialization (the proposed initialization, and that of Liu (Liu et al. 2019)) shows a significant improvement in the test accuracy of Scratch, and RigL or our proposed initialization, although not quite reaching lottery or RigL accuracy. Finally, we see no significant effect on SET training, with none of the initialization variants having a significant increase over any of the others, although the Liu (Liu et al. 2019) initialization does marginally better.

The gradient flow of this model is shown in Fig. 9. While we see moderate improvements to Scratch gradient flow early on in training with our proposed initialization (a), RigL shows significantly higher gradient flow throughout training, in particular after mask updates (b), mirroring the results of LeNet5. The interpolation graphs in (c) only differ slightly from that of LeNet5, again showing that our results for LeNet5 broadly hold for the fully-connected model.

E Hessian Spectrum of LeNet5

Given a loss function L and parameters θ , we can write the first order Taylor approximation of the change in loss $\Delta L = L(\theta^{t+1}) - L(\theta^t)$ after a single training step with the learning rate $\epsilon > 0$ as :

$$\Delta L \approx -\epsilon \nabla L(\theta)^T \nabla L(\theta). \quad (31)$$

Note that as long as the error is small, gradient descent is guaranteed to decrease the loss by an amount proportional to $\nabla L(\theta)^T \nabla L(\theta)$, which we refer as the *gradient flow*. In practice large learning rates are used, and the first order approximation might not be accurate. Instead we can look at the second order approximation of ΔL :

$$\Delta L \approx -\alpha \nabla L(\theta)^T \nabla L(\theta) + \frac{\alpha^2}{2} \nabla L(\theta)^T H(\theta) \nabla L(\theta), \quad (32)$$

where $H(\theta)$ is the Hessian of the loss function. The eigenvalue spectrum of Hessian can help us understand the local

landscape (Sagun et al. 2017), and help us identify optimization difficulties (Ghorbani, Krishnan, and Xiao 2019). For example, if and when the gradient is aligned with large magnitude eigenvalues, the second term of Eq. (32) can have a significant effect on the optimization of L . If the gradient is aligned with large positive eigenvalues, it can prevent gradient descent from decreasing the loss and harm the optimization. Similarly, if it is aligned with negative eigenvalues it can help to accelerate optimization.

We show the Hessian spectrum before and after the topology updates in Fig. 10. After RigL updates we observe new negative eigenvalues with significantly larger magnitudes. We also see larger positive eigenvalues, which disappear after few iterations**. In comparison, the effect of SET updates on the Hessian spectrum seems limited.

We also evaluate the Hessian spectrum of LeNet5 during the training. In Fig. 11b, we observe similar shapes for each method on the positive side of the spectrum, however, on the negative side dense models seem to have more mass. We plot the magnitude of the largest negative eigenvalue to characterize this behaviour in Fig. 11a. We observe a significant difference between sparse and dense models and observe that sparse networks trained with RigL have larger negative eigenvalues.

F Comparing Function Similarity

Table 7 gives a full list of comparison metrics of the predictions on the test set for LeNet5 on MNIST and ResNet50 on ImageNet-2012, in particular here we also compare the output probability distributions using relevant metrics.

Fort, Hu, and Lakshminarayanan (2020) motivate deep ensembles by empirically showing that models starting from different random initializations typically learn different solutions, as compared to models trained from similar initializations. Here we adopt the analysis of (Fort, Hu, and Lakshminarayanan 2020), but in comparing LT initializations and random initializations using *fractional disagreement* — the fraction of class predictions over which the LT and scratch models disagree with the pruning solution they were derived from. In Table 7 we show the mean fractional disagreement over all pairs of models. We run two versions of scratch training: (1) *Scratch (Diff. Init.)* different weight initialization and different data order (2) *Scratch* same weight initialization and different data order for 5 different seeds the experiments are ran. Finally, we restart training starting from the pruning solution (*Prune Restart*) using, again, 5 different data orders.

The results presented in Table 7 suggest that all 5 LTs models converge on a solution almost identical to the pruning solution. Interestingly, the 5 LT models are even more similar to each other (*Disagree.* column) than the pruning solution, possibly because they share an initialization and training is stable (Frankle et al. 2019). The disagreement of *Prune Restart* solutions with the original pruning solution matches the disagreement of lottery solutions; showing the extent of similarity between LT and pruning solutions.

Our results show that having a fixed initialization alone can not explain the low disagreement observed for LT experi-

**We share videos of these transitions in supplementary material.

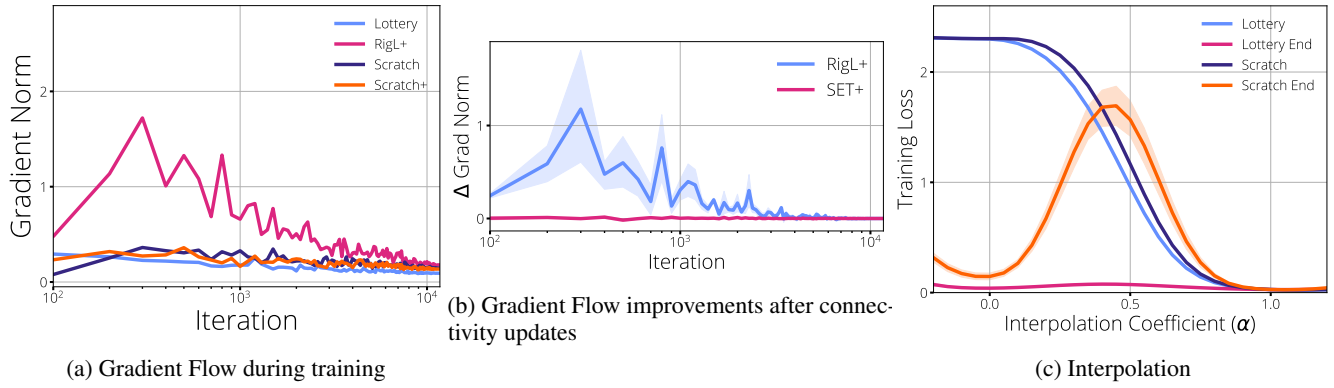


Figure 9: **Sparse 300-100 MLP experiments.** Gradient flow during training averaged over multiple runs, ‘+’ indicates training runs with our proposed sparse initialization.

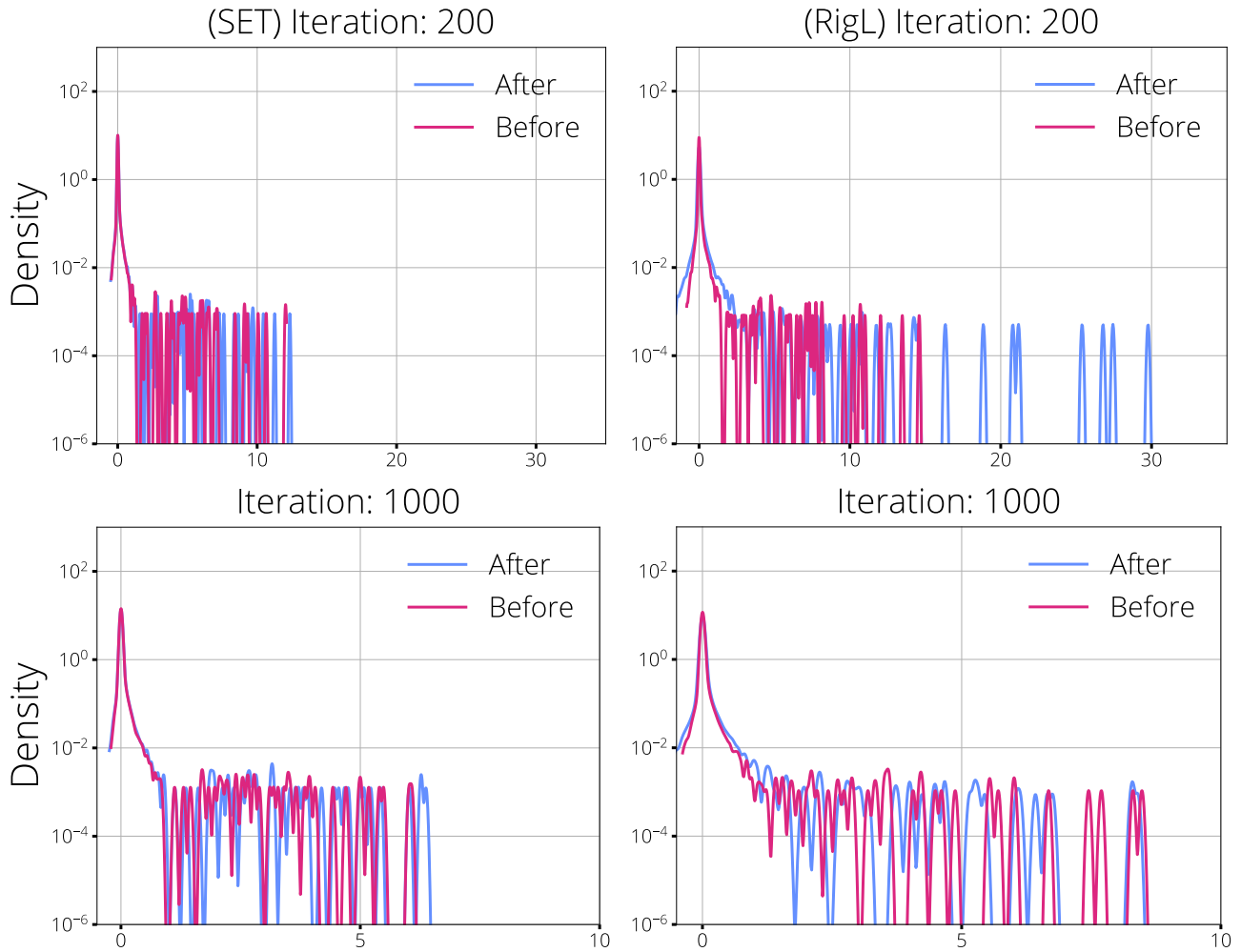
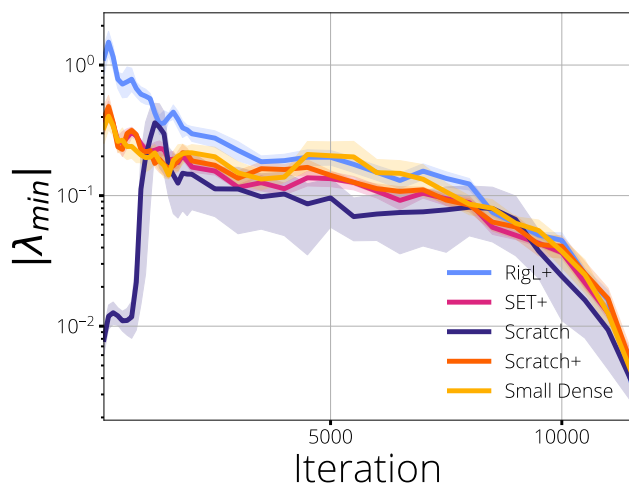
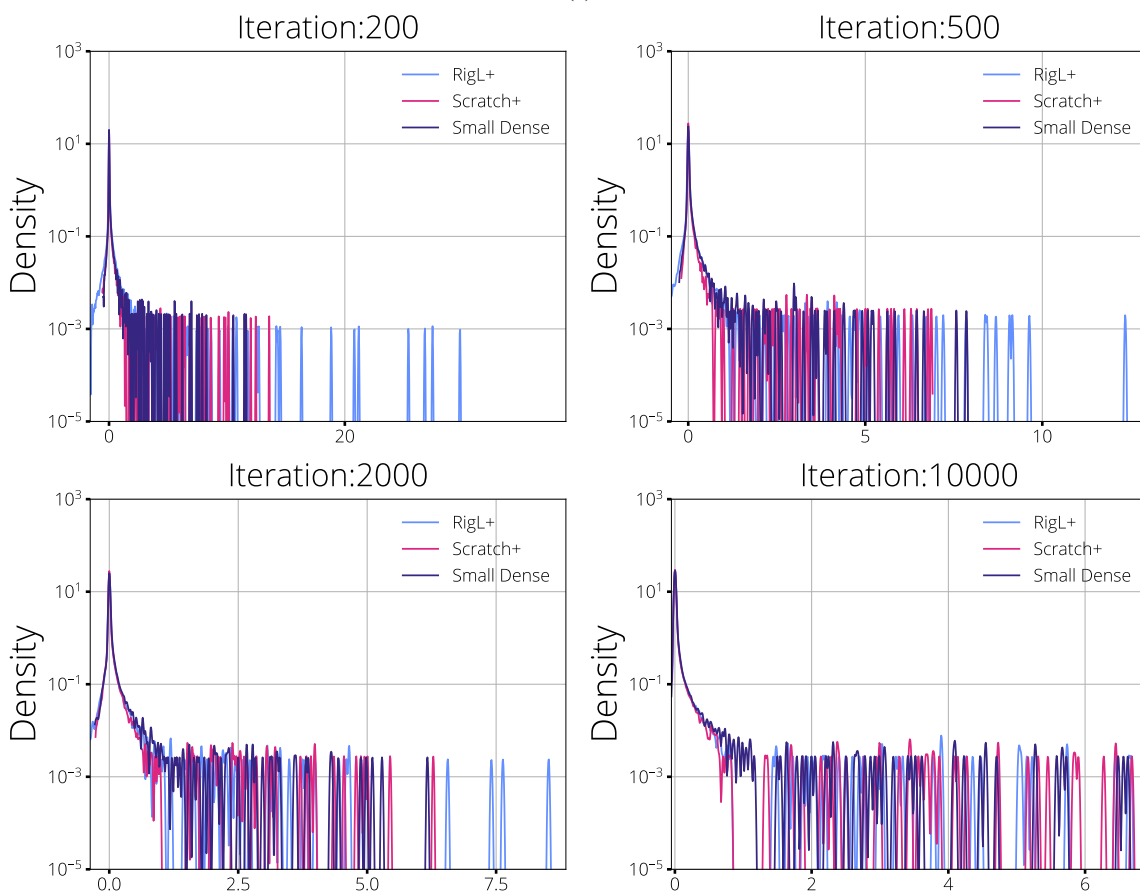


Figure 10: Hessian spectrum before and after mask updates: **(left)** SET **(right)** RigL. Similar to (Ghorbani, Krishnan, and Xiao 2019), we estimate the spectral density of Hessian using Gaussian kernels.



(a)



(b)

Figure 11: MNIST Hessian spectrum experiments.

Table 7: **Ensemble/Prediction Disagreement.** In order to show the function similarity of LTs to the pruning solution, we follow the analysis of (Fort, Hu, and Lakshminarayanan 2020), and compare the function similarity and ensemble generalization over 5 sparse models trained using random initializations and LTs with the original pruning solution they are derived from. The fractional disagreement is the pairwise disagreement of class predictions over the test set, as compared within the group of sparse models, and as compared to the pruned model whose mask they were derived from. KL and JSD compare the prediction distributions over all the test samples.

MNIST/LeNet5										
Init. Method	Test Acc. (Top-1)	Ensemble	Pairwise Disagree.	Disagree. w/ Pruned	Pairwise KL	KL w/ Pruned	5-model JSD	JSD w/ Pruned		
Pruned Soln.*	98.53	—	—	—	—	—	—	—		
LT	98.52 ±0.02	98.58	0.0043±0.0006	0.0089±0.0002	0.0030±0.0004	0.0039±0.0028	0.0140 ±0.0004	0.0033±0.0001		
Scratch	97.04 ±0.15	98.00	0.0316±0.0023	0.0278±0.0020	0.0917±0.0126	0.0506±0.0238	0.1506 ±0.0130	0.0159±0.0009		
Scratch (Diff. Init.)	97.19 ±0.33	98.43	0.0352±0.0037	0.0278±0.0032	0.1358±0.0202	0.0650±0.0301	0.1468 ±0.0295	0.0157±0.0021		
Prune Restart	98.60 ±0.01	98.63	0.0027±0.0003	0.0077±0.0003	0.0014±0.0001	0.0019±0.0014	0.0105 ±0.0001	0.0027±0.0000		
Pruned w/ Diff. Init.**	98.30 ±0.23	99.07	0.0214±0.0023	0.0197±0.0019***	0.0741±0.0107	0.0438±0.0241	0.0752 ±0.0133	0.0103±0.0010		
Init. Method	Test Acc. (Top-1)	Ensemble	Pairwise Disagree.	Disagree. w/ Pruned	Pairwise KL	KL w/ Pruned	5-model JSD	JSD w/ Pruned		
ImageNet-2012/ResNet-50										
Pruned Soln.*	0.7554	—	—	—	—	—	—	—		
LT	75.730±0.008	76.27	0.0894±0.0008	0.0941±0.0009	3325.0±26.4	3605.0±12.4	787.20±5.24	853.70±3.55		
Scratch	71.16 ±0.13	74.05	0.2039±0.0013	0.2033±0.0012	15 787 ±105	20 442 ±178	3316.0 ±13.2	3847.0 ±26.0		
Pruned w/ Diff. Init.**	75.65 ±0.13	77.78	0.1620±0.0008	0.1623±0.0011***	13 158 ±143	13 087.0±55.9	2760.0 ±16.8	2755.00±4.96		

* This is the pruning solution that the LT and scratch models are derived from.

** 5 pruning solutions found with different random initialization, one of which is the pruning solution above.

*** Here we compare 4 different pruned models with the pruning solution the LT/Scratch are derived from.

ments as *Scratch* solutions obtain an average disagreement of 0.0316 despite using the same initialization, which is almost 10 times more than the LT solutions (0.0043). Finding different LT initialization is costly, however using a different initialization in *Scratch (Diff. Init.)* training is free as the initializations are random. Using different initializations we can obtain more diverse solutions and thus achieve higher ensemble accuracy. As suggested by the analysis of Fort, Hu, and Lakshminarayanan (2020), ensembles of different solutions are more robust, and generalize better, than ensembles of similar solutions. An ensemble of 5 LT models with low disagreement doesn't significantly improve generalization as compared to an ensemble of 5 different pruning solutions with similar individual test accuracy. We further demonstrate these results by comparing the output probability distributions using the KL, and JSD.